Solution of the radial Schrödinger equation in cylindrical and spherical coordinates by mapped Fourier transform algorithms

Article *in* The Journal of Chemical Physics · May 2001

DOI: 10.1063/1.1358867

CITATIONS
30

READS
158

1 author:

Andrey Borissov
French National Centre for Scientific Research
228 PUBLICATIONS **6,754** CITATIONS

SEE PROFILE

Solution of the radial Schrödinger equation in cylindrical and spherical coordinates by mapped Fourier transform algorithms

A. G. Borisov
Laboratoire des Collisions Atomiques et Moléculaires, Unité Mixte de Recherche CNRS-Université Paris-Sud UMR 8625, Bâtiment 351, Université Paris-Sud, 91405 Orsay Cedex, France

(Received 21 November 2000; accepted 5 February 2001)

When used in the on-the-grid solvers of the stationary or time-dependent Schrödinger equation, coordinate mapping allows one to achieve a very accurate description of the wave function with an optimal number of the grid points. The efficiency of the mapped Fourier grid methods has been recently demonstrated by V. Kokoouline, O. Dulieu, R. Kosloff, and F. Masnou-Seeuws [J. Chem. Phys. **110**, 9865 (1999)] and by D. Lemoine [Chem. Phys. Lett. **320**, 492 (2000)]. In this paper we propose a discrete coordinate representation based on a numerical mapping in cylindrical and spherical coordinates. Within proposed approach, the Hamiltonian matrix is Hermitian, and the use of the fast cosine and sine Fourier transforms provides a very efficient way of calculating the Laplacian operator. © *2001 American Institute of Physics.* [DOI: 10.1063/1.1358867]

I. INTRODUCTION

The accurate representation of the wave function on a grid of points is one of the main problems of the time-dependent or stationary methods for the solution of the Schrödinger equation. Development of the pseudospectral global grid representation approaches yielded a very efficient way to tackle this problem.[1] The discrete variable representation (DVR) method[2–4] and the Fourier grid Hamiltonian method (FGH) (Refs. 5, 6) have been widely used in time-dependent molecular dynamics,[7–9] as well as in stationary S-matrix[10–13] or eigenvalue[14–16] calculations. The advantage of the FGH method based on the Fast Fourier Transform (FFT) algorithm is that for the mesh of N points the evaluation of the kinetic energy operator requires $N \log N$ operations and can be easily implemented numerically. In the standard FGH method the sought wave function is represented on a grid of equidistant points in coordinate or momentum space.[5–7] This is well suited for the case where the phase space of the problem is close to rectangular shape, i.e., where the local de Broglie wavelength does not change much over the physical region spanned by the wave function of the system.[7,17] There are, however, a lot of examples where the system under consideration spans the physical regions with very different properties and so has an essentially non rectangular shape of the phase space. This is why much of work has been devoted recently to the development of the FGH schemes that implement the coordinate mapping in order to enhance sampling efficiency in the regions of rapid variations of the wave function.[7,17–23] Most of the proposed methods rely on analytical mapping procedure.[7,17–21] Only recently completely numerical mapping has been proposed which is perfectly adapted to the local de Broglie wavelength of the sought wave function.[22,23]

The common wisdom is that the mapping procedure complicates the evaluation of the Laplacian operator, even rendering its matrix non-Hermitian in the FGH representation.[17,21–23] Special procedures have been proposed to symmetrize the Laplacian operator in the new coordinates in order to retrieve Hermiticity in FGH representation.[21–24] The price to pay is extra-potential terms in the resulting Hamiltonian. These might be fast-varying and large, and might degrade the convergence of, e.g., eigenvalue calculations.[21,23] At this point it should be noted that setting up a procedure that leads to Hermitian Hamiltonian matrix in FGH is not always necessary since a very accurate description of the bound states can be obtained with non-Hermitian schemes.[17,21,23] At the same time it is desirable since it allows one to use efficient diagonalization techniques for the eigenvalue determination and implicitly norm-conserving propagators in dynamical wave packet propagation studies.

In this paper we present an approach which allows one to deal with singularities in the radial parts of the Schrödinger equation in cylindrical and spherical coordinates and has several attractive properties: (i) The numerical coordinate mapping is performed which leads to the efficient description of the wave function; (ii) The fast sine and cosine Fourier transforms are implemented for the evaluation of the Laplacian operator; (iii) The discrete coordinate representation of the Hamiltonian matrix is Hermitian while no extra-potential terms is included. We illustrate this method on the examples of the harmonic oscillator in cylindrical coordinates and Coulomb problem in cylindrical and spherical coordinates. Atomic units are used throughout the paper unless otherwise stated.

II. MAPPED FOURIER METHOD IN CYLINDRICAL COORDINATES

A. General presentation

The major problem in the cylindrical coordinates is the correct description of the radial dependence of the wave function close to the origin.[21,25–27] Therefore, we will limit our discussion to the one-dimensional radial case, though the

method presented below is not restricted to one dimension. The radial Schrödinger equation in cylindrical coordinates reads

$$\left[-\frac{1}{2}\frac{1}{\rho}\frac{d}{d\rho}\rho\frac{d}{d\rho}+\frac{m^2}{2\rho^2}+V\right]\Psi=E\Psi, \tag{1}$$

where m stands for the magnetic quantum number and V is a potential. Usually the wave function is scaled according to $\Psi=\tilde{\Psi}/\sqrt{\rho}$, and Eq. (1) transforms into

$$\left[-\frac{1}{2}\frac{d^2}{d\rho^2}+\frac{m^2-1/4}{2\rho^2}+V\right]\tilde{\Psi}=E\tilde{\Psi}. \tag{2}$$

The advantage of the form (2) is that, the second derivative can be easily evaluated with the FGH technique.[13,24] As it was discussed in the literature, the unmapped discrete coordinate methods based on the sine transform are poorly suited for the cylindrical coordinate case.[21,25,26] Even though the attractive singularity at the origin is removed already for $m=1$, a reasonable description of the sought wave function can be obtained only for $m>1$. The most difficult is the $m=0$ case. Consider, e.g., the harmonic oscillator ($V=\rho^2/2$); close to the origin the divergent term $-(1/8\rho^2)$ has to be compensated by the second derivative of the wave function. Then the wave function behaves like $\sqrt{\rho}$, which is difficult to describe with a $\sin(k\rho)$ basis set. The natural choice in this case is the discretization of Eq. (1) with the DVR basis formed by the Bessel functions. This solves analytically the divergence at the origin, and leads to an excellent accuracy in the eigenenergies.[25–27] On the other hand, for the time-dependent studies, one loses an advantage of the reduced number of operation in calculating the Laplacian operator as provided by Fourier grid methods. Another solution consists in extending the grid to negative ρ and using the FGH method with coordinate mapping to densify the points on the physical grid close to $\rho=0$.[17] An elegant method, using the coordinate mapping and discrete sine Fourier transform has been proposed recently in Ref. 21. The disadvantage of the latter two approaches is that the best results were obtained for a non-Hermitian discrete form of the Hamiltonian matrix. Moreover, the approach proposed in Ref. 21 is limited to the power law mapping procedure $\rho=x^n$. This might be a disadvantage since, for a fixed step size Δ on the working grid x_i, the step size $\Delta\rho$ on the physical grid is continuously increasing with increasing ρ: $\Delta\rho=n\rho^{1-(1/n)}\Delta$. This does not necessarily correspond to the local behavior of the de Broglie wavelength over the entire region spanned by the wave function which might reduce the sampling efficiency.

Here we propose an alternative procedure. Starting from Eq. (1) with a general mapping function $\rho=f(x)(f(0)=0)$ we obtain

$$\left[-\frac{1}{2}\frac{1}{fJ}\frac{d}{dx}\frac{f}{J}\frac{d}{dx}+\frac{m^2}{2f^2}+V\right]\Psi=E\Psi, \tag{3}$$

where J is the Jacobian of the transformation: $J(x)=df/dx$. When scaling the wave function with $\Psi=\Phi/\sqrt{fJ}$ this equation takes the form of

$$\left[-\frac{1}{2}\frac{1}{\sqrt{fJ}}\frac{d}{dx}\frac{f}{J}\frac{d}{dx}\frac{1}{\sqrt{fJ}}+\frac{m^2}{2f^2}+V\right]\Phi=E\Phi. \tag{4}$$

Equation (4) forms the basis of the proposed method. Owing to the symmetric form of the Laplacian operator, the discretization procedure leading to a Hermitian Hamiltonian matrix can be easily derived.

The discrete form of Eq. (4) is obtained along the lines of Refs. 6, 7, 21, 24. For a grid of N equally spaced points $x_i=\frac{1}{2}\Delta+(i-1)\Delta$ $(i=1,...,N)$ the discrete form of a function $F(x)$ is obtained as $F_i=F(x_i)$. Fast sine and cosine transforms of the second type[28,29] are used to switch between the coordinate and momentum space,

$$C_k=\alpha_k\sum_{m=1}^{N}F_m\cos\left[\frac{2m-1}{2N}k\pi\right],\quad k=0,...,N-1,N, \tag{5a}$$

$$F_m=\frac{2}{N}\sum_{k=0}^{N-1}\alpha_k C_k\cos\left[\frac{2m-1}{2N}k\pi\right],\quad m=1,...,N, \tag{5b}$$

and

$$S_k=\alpha_k\sum_{m=1}^{N}F_m\sin\left[\frac{2m-1}{2N}k\pi\right],\quad k=0,1,...,N, \tag{6a}$$

$$F_m=\frac{2}{N}\sum_{k=1}^{N}\alpha_k S_k\sin\left[\frac{2m-1}{2N}k\pi\right],\quad m=1,...,N, \tag{6b}$$

where

$$\alpha_k=\begin{cases}1/\sqrt{2}, & k=0,N,\\ 1, & \text{otherwise.}\end{cases} \tag{7}$$

Note that we have added the zero components to the **C** and **S** vectors of coefficients in Eqs. (5a) and (6a); these are C_N and S_0. This is done uniquely in order to have compact formulations of the discretized form of the Laplacian operator as presented below. An operator form of the Eqs. (5) and (6) can be defined as

$$\mathbf{C}=\hat{A}_{\cos}\mathbf{F}, \tag{8a}$$

$$\mathbf{F}=(\hat{A}_{\cos})^{-1}\mathbf{C}, \tag{8b}$$

and

$$\mathbf{S}=\hat{A}_{\sin}\mathbf{F}, \tag{9a}$$

$$\mathbf{F}=(\hat{A}_{\sin})^{-1}\mathbf{S}. \tag{9b}$$

Within the discrete coordinate representation the vector **F** corresponds to the representation of the wave function $F(x)$ within the basis set of functions φ_j defined on the grid points as

$$\varphi_j(x_i)=\delta(x_i-x_j)\quad (i,j=1,...,N). \tag{10}$$

The $\hat{A}_{\cos}$ and $\hat{A}_{\sin}$ give the transformation between the discrete basis φ_j in coordinate space and the discrete basis of sine or cosine functions in momentum space. In the φ_j basis the potential and Laplacian operators are represented by $N\times N$ matrices and the eigenvalues and eigenvectors of the Hamiltonian are obtained by matrix diagonalization. The po-

tential energy operator is assumed to be diagonal in the φ_j representation[2] and is given by $V_{kn}=V(x_k)\delta_{kn}$ $(k,n=1,...,N)$. The matrix of the Laplacian operator has to be calculated numerically. Let

$$\hat{L}=\frac{1}{\sqrt{fJ}}\frac{d}{dx}\frac{f}{J}\frac{d}{dx}\frac{1}{\sqrt{fJ}}-\frac{m^2}{f^2},$$

then the discrete form can be obtained as

$$L_{kn}=-[\mathbf{B}(\hat{A}_{\cos})^{-1}\mathbf{K}\hat{A}_{\sin}\mathbf{R}(\hat{A}_{\sin})^{-1}\mathbf{K}\hat{A}_{\cos}\mathbf{B}\Xi(\mathbf{n})]_k - \frac{m^2}{f(x_k)^2}\delta_{kn} \quad (k,n=1,...,N), \tag{11}$$

where the action of the $\hat{A}_{\cos}$ and $\hat{A}_{\sin}$ operators is defined by Eqs. (5)–(9). **B**, **R**, and **K** are the diagonal matrixes given by

$$B_{ij}=\frac{1}{\sqrt{f(x_i)J(x_i)}}\delta_{ij}, \quad R_{ij}=\frac{f(x_i)}{J(x_i)}\delta_{ij} \quad (i,j=1,...,N), \tag{12}$$

$$K_{ij}=\frac{\pi i}{N\Delta}\delta_{ij} \quad (i,j=0,1,...,N). \tag{13}$$

The K_{ij} matrix elements correspond to the plane wave wave vectors. The $\Xi(\mathbf{n})$ is the vector defined as $\Xi(n)_i=\delta_{in}$ $(i=1,...,N)$.

The problem of the divergence at the origin $[f(0)=0]$ is avoided by using sine and cosine transforms of the second type with grid points which not include the $x=0$ point. The order of the cosine and sine transforms in Eq. (11) is particularly well suited to account for the boundary condition $(x=0)$ for the sought wave function $\Psi=\Phi/\sqrt{fJ}$ in the $m=0$ and $m>1$ cases, $d\Psi/dx=0$. Below we demonstrate that discretization given by Eq. (11) can be also successively applied in the $m=1$ case.

One can show that the Hamiltonian matrix $(H_{kn}=-\frac{1}{2}L_{kn}+V_{kn})$ obtained in this way is real and symmetric (Hermitian). This is achieved without inclusion of any extra-potential terms. The efficient diagonalization techniques can be applied for the eigenvalue determination. Moreover, in case of the time-dependent studies, implicitly norm-conserving propagators can be used. Note, that we consider the general mapping function $f(x)$, it can be defined analytically or numerically. Within the present approach four Fast Fourier operations are required to evaluate the action of the Laplacian operator. This is to be compared with two Fast Fourier operations for the unmapped methods. Four FFT operations are also required in the method of coordinate mapping with Laplacian symmetrization through the inclusion of extra-potential terms.[21–24] Within the latter method, the matrix elements of the Hamiltonian in discrete coordinate representation can be obtained analytically[21–24,30] which is an advantage. The disadvantage consists in the essential loss of precision in the eigenvalue determination because of the extra-potential terms (see discussion in Refs. 21 and 23). We believe that the numerical evaluation of the Hamiltonian matrix in discrete coordinate representation employed here should not be a shortcoming of the method since fast sine and cosine transforms are readily available in most of the modern computer libraries.

B. The mapping procedure

The standard FGH method with a constant grid step h samples the rectangular phase space with maximum wave vector given by $k_{\max}=\pi/h$.[7,17] The idea of the mapping is to adapt the phase space sampling to the physical problem at hand.[17,22,23] This can be achieved by introducing a local step on the physical grid depending on the local de Broglie wavelength of the wave function, i.e., on the local kinetic energy. An efficient choice of the local step $\Delta(\rho)$ is given by[22,23]

$$\Delta(\rho)=\frac{\alpha\pi}{\sqrt{2(W-U(\rho))}}, \tag{14}$$

where W represents the energy of the problem, $U(\rho)$ will be called the ''generating potential'', and α is an adjustable parameter $(\alpha<1)$ which serves to control the density of the grid points. The $U(\rho)$ can be also used to set the maximum step size in the classically forbidden region in order to correctly reproduce the exponential tail of the wave function.[22] The variable transformation $\rho=f(x)$ relates the constant step Δ on the working grid x_i $(i=1,...,N)$ and a variable step $\Delta[\rho(x)]$ on the physical grid through

$$\Delta(\rho)=\frac{df}{dx}\Delta=\frac{\alpha\pi}{\sqrt{2[W-U(\rho)]}}. \tag{15}$$

For a given choice of the generating potential $U(\rho)$ the $f(x_i)$ function can be obtained by numerically solving Eq. (15) by, e.g., Runge–Kutta propagation with initial condition $f(0)=0$. In practice, we do not use directly the result of the numerical solution of Eq. (15), but we first perform a sine Fourier transform of it, apply a Gauss filter (typically of the width $\pi/8\Delta$) in the momentum space, and then back transform. This is done to remove the high momentum components in $f(x)$ and, especially, in its high order derivatives so that the $f(x)$ and $J(x)$ functions actually used in the calculation are sufficiently smooth and well represented within the Fourier basis.[23] The $J(x)$ can be obtained from $f(x)$ with the help of the differentiation procedure based on the fast sine and cosine Fourier transforms.

C. The 2D harmonic oscillator

First, we consider the case of the 2D harmonic oscillator $(V=\rho^2/2)$. Even though the diverging at the origin term $-(1/8\rho^2)$ [see Eq. (2)] is not appearing explicitly in the symmetrized form of the Laplacian operator given by Eq. (4), it is implicitly present through the wave function scaling $\Psi=\Phi/\sqrt{\rho J}$, where $\rho=f(x)$. Therefore we use the following form of the generating potential in the mapping procedure,

$$U=-\frac{1}{8}\frac{1}{(\rho+\epsilon)^2}, \tag{16}$$

where $\epsilon=10^{-20}$ is used here to remove the divergence at the origin in the Runge–Kutta solution of Eq. (15). It is worth mentioning that, for $W=0$ and $\epsilon=0$, the solution of Eq. (15)

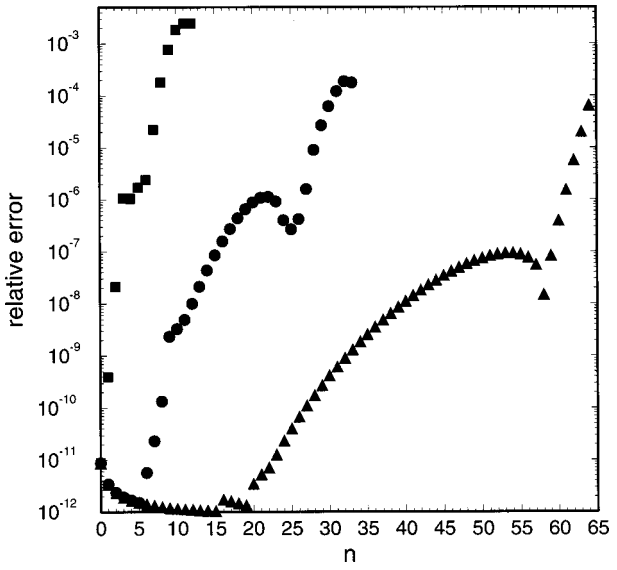

FIG. 1. Radial Schrödinger equation in cylindrical coordinates, harmonic oscillator problem. Relative error in the eigenvalue calculation for the $m=0$ states as function of the radial quantum number n. Different symbols correspond to different numbers N of the grid points used in the calculation. Squares, $N=32$; dots, $N=64$; triangles, $N=128$.

is an exponential function. As discussed in the literature,[23,24] the exponential scaling might be very efficient in solving the Coulomb problem.

In the present calculation, W was adjusted in order to correctly reproduce the behavior of the wave function corresponding to the largest eigenvalues that were looked for: $W \cong E_n^{\max}$. Here, n is the radial quantum number ($n=0,1,...$) and E_n is the energy of the nth state of the harmonic oscillator: $E_n=1+2n$. The calculations were performed for the $m=0$ case, where the unmapped schemes give poor results with a very slow convergence.

In Fig. 1 we show the modulus of the relative error of the eigenvalue calculation. The results are obtained with $N=32$, 64, and 128 grid points. All calculations were performed for the stepsize on the working grid $\Delta=1$, and $\alpha=0.8$. The W parameter was adjusted in each case as explained above leading to the $W_{32}=18$, $W_{64}=55$, and $W_{128}=150$ values actually used in the calculations. With this choice of parameters the physical space $0 \leqslant \rho \leqslant L$ spanned in the three cases depends on N and corresponds to $L_{32}=7.67$, $L_{64}=12.08$, and $L_{128}=16.62$. For $N=32$ grid points, nine states can be obtained with at least four significant digits of precision. Precision can reach up to 11 significant digits for the lowest state. These results are quite comparable with results obtained by Lemoine with the analytical $\rho=x^2$ mapping and a non-Hermitian representation of the Laplacian operator,[21] where 12 eigenvalues are reproduced with a relative error on the 10^{-4} level. The slightly larger number of states obtained with the analytical mapping is because of the smaller density of the points on the physical grid close to the origin compared to the present method. Then a larger number of points on the working x-grid *might be* needed in the present method to have the same extension of the physical ρ-grid in order to represent the same number of bound states. At the same time, the lowest eigenstates are obtained with a much higher precision (at least by three orders of magnitude) in the present method. This is once again a consequence of the higher density of physical grid points close to the origin.

Impressive results can be obtained if one considers a large number of eigenstates. With the present method, due to the optimized step size in the physical grid ρ far from the origin, the number of grid points per state can be much reduced. Indeed, for $N=32$ one needs 3 points per state, while only 2 points per state are needed for $N=64$ and $N=128$. Note the extremely large precision at which up to 60 states of the harmonic oscillator can be found for $N=128$. This is an advantage when compared to the analytical mapping procedure,[21] where the step size on the physical grid is not necessarily optimized to describe the wave function behavior over the large ρ-region. At this point it is important to note that the unmapped schemes based on the Bessel function expansion of the sought wave function[25–27] also give extremely good results in the harmonic oscillator case. Thus, 15 eigenvalues can be obtained with at least 10 significant figures for $m=0$ and using the $N=32$ point grid.

The advantage of the numerical mapping is more transparent in case of the Coulomb problem where the extensions of the wave functions of the different states can vary by orders of magnitude. Moreover the wave functions of the high Rydberg states ''probe'' ρ-regions with extremely different strengths of the potential.

D. The 2D Coulomb case

We consider the 2D Coulomb case: $V=-1/\rho$, where the energies of the bound states are given by the analytical expression, $E_{nm}=-0.5/(m+0.5+n)^2$. In this case we chose a generating potential including the Coulomb term and equal to

$$U=-\frac{1}{8}\frac{1}{(\rho+\epsilon)^2}-\frac{1}{(\rho+\epsilon)}, \tag{17}$$

where the ϵ-parameter was discussed in Sec. II C. Since we are interested in the Rydberg series with energies of the states converging towards the vacuum limit, the W parameter in Eq. (15) is set to zero.

In Fig. 2 we summarize results obtained for the $m=0$ with different number of points N on the working grid and for various choices of the step size Δ and of the α parameter (see figure caption for further details). With $N=32$ points we obtain 13 eigenvalues with a precision of 4 significant figures or better so that about 2.5 grid points per state are needed. The results obtained in Ref. 21 with $N=32$ grid points and $\rho=x^3$ analytical variable change were slightly better even though the precision at which the first two states are obtained is several orders of magnitude better in the present approach. The higher efficiency of the power law variable change for the grids with small N can be explained by the lower density of the sampling points on the physical grid close to the origin (see Sec. II C).

The advantage of the numerical variable change reveals when the highly excited states have to be calculated. Thus, increasing the number of points from $N=32$ to $N=128$, and

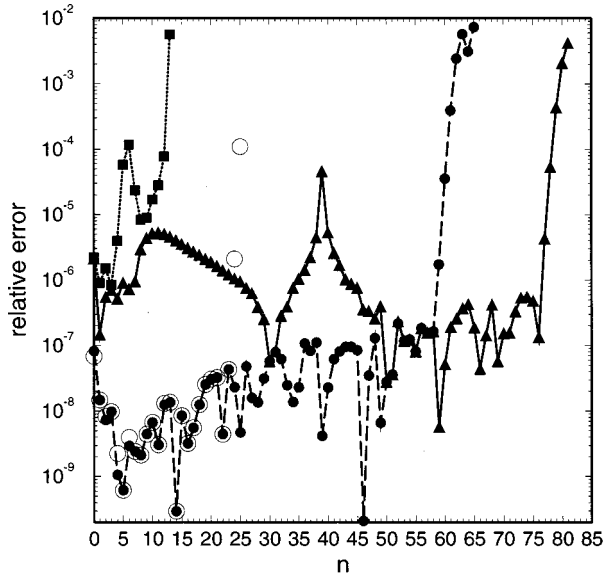

FIG. 2. Radial Schrödinger equation in cylindrical coordinates, Coulomb problem. Relative error in the eigenvalue calculation for the $m=0$ states as function of the radial quantum number n. Different symbols correspond to different values for the number of grid points N, the Δ and α parameters entering Eq. (15), and the extension of the physical grid L, $0<\rho<L$. Squares with dotted line, $N=32$, $\Delta=1.25$, $\alpha=0.9$, $L=393$; open circles, $N=64$, $\Delta=1$, $\alpha=0.72$, $L=1501$; dots with dashed line, $N=128$, $\Delta=1$, $\alpha=0.72$, $L=8003$; triangles with solid line, $N=128$, $\Delta=1.25$, $\alpha=0.9$, $L=13\,170$.

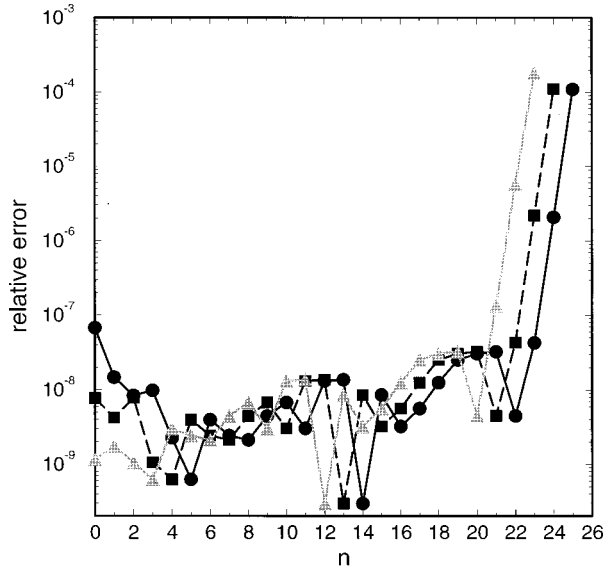

FIG. 3. Radial Schrödinger equation in cylindrical coordinates, Coulomb problem. Relative error in the eigenvalue calculation for the different m-states as function of the radial quantum number n. Dots with solid line: $m=0$; squares with dashed line: $m=1$; gray triangles with solid line: $m=2$. Calculation is performed with $N=64$ points on the grid. The choice of the Δ and α parameters for $N=64$ is given in the caption for Fig. 2.

keeping the same Δ and α parameters, 79 states can be obtained with at least four significant figures. This corresponds to 1.6 grid points used per state. Note that the energy ratio between the highest and lowest states, $E_{n=78}/E_{n=0}=4\times10^{-5}$ reflects the extremely different ρ-ranges probed by these two states. Owing to the numerical variable change based on the local de Broglie wavelength, one can achieve the optimal density of the grid points allowing a good representation of both the $n=0$ and $n=78$ states. Decreasing the step size from 1.25 to 1 and keeping the same α/Δ ratio improves the overall precision by several orders of magnitude as seen in the figure. At the same time less states for the same N can be calculated because of the smaller L size of the physical grid.

As it was already discussed, the order of the sine and cosine transforms in Eq. (11) is well adapted to treat the $m=0$ and $m>1$ cases. Reversed order of the sine and cosine transforms might be preferred for $m=1$ to better reproduce the boundary condition at $\rho=0$. Nevertheless, the discretization given by Eq. (11) still can be successfully applied. In Fig. 3 we present the results obtained with $N=64$ points grid for different m ($m=0,1,2$). In all three cases at least 21 states are reproduced with at least seven significant digits. The relative error of the eigenvalue calculation is quite uniform over m.

In Fig. 4 we illustrate the procedure of numerical mapping. The $f(x)$ and $J(x)$ functions are shown. Due to the very small step size on the physical grid close to the origin of the physical grid; $\Delta\rho|_{\rho=f(x)}=J(x)\Delta$ the sharp behavior of the Coulomb wave functions close to the origin on the physical grid is smoothed out on the working grid. This allows efficient description of the sought wave function Ψ in the cosine basis.

III. MAPPED FOURIER METHOD IN SPHERICAL COORDINATES

A. General

In this section the general approach to the mapping procedure presented in this paper is illustrated on the example of the hydrogenlike Coulomb problem. This problem was treated previously by Fattal and Kosloff by the FGH method

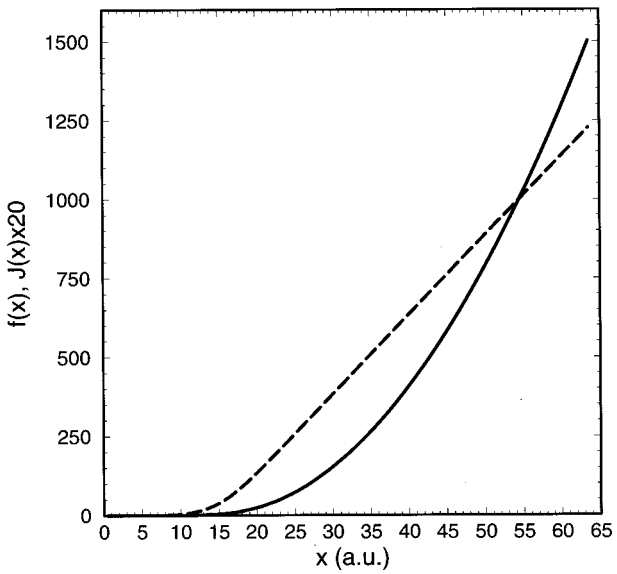

FIG. 4. Mapping functions calculated from Eq. (15) with $\Delta=1$, $\alpha=0.72$, and $W=0$ for the Coulomb problem treated on the $N=64$ points grid. Solid line, $f(x)$; dashed line, $J(x)$.

with an extension of the radial coordinate to the negative axis, and with an analytical mapping procedure leading to a non-Hermitian Hamiltonian matrix.[17] Later, Kokooline and Kosloff treated the same problem with the FGH method and numerical mapping on the positive axis.[23] Symmetrized and nonsymmetrized Laplacian operator cases were considered with symmetrization procedure involving the extra-potential terms.

The wave function scaling $\Psi=\tilde{\Psi}/r$ transforms the radial Schrödinger equation for the Coulomb problem to the form,

$$\left(-\frac{1}{2}\frac{d^2}{dr^2}-\frac{Q}{r}+\frac{l(l+1)}{2r^2}\right)\tilde{\Psi}=E\tilde{\Psi}, \tag{18}$$

where Q is the Coulomb charge and l stands for the angular momentum. We will consider only the $l=0$ case which is the most difficult one because of the divergent attractive term at the origin.[17] With general mapping function $r=f(x)$ $[f(0)=0]$ and the wave function scaling $\tilde{\Psi}=\Phi/\sqrt{J(x)}$, Eq. (18) transforms to

$$\left(-\frac{1}{2}\frac{1}{\sqrt{J}}\frac{d}{dr}\frac{1}{J}\frac{d}{dr}\frac{1}{\sqrt{J}}-\frac{Q}{f}\right)\Phi=E\Phi, \tag{19}$$

where $J(x)$ is the Jacobian of transformation $J(x)=df/dx$. As in the case of the radial Schrödinger equation in cylindrical coordinates [Eq. (4)] the Laplacian operator is given by a symmetric form so that the discretization procedure can be defined leading to a Hermitian Hamiltonian matrix and employing fast sine and cosine transforms. Because of the zero boundary condition at the origin the description of the wave function in the basis of sine functions is well suited in the present case. In what follows below we will use the discrete direct and inverse cosine and sine transforms of the first kind to switch between the coordinate and momentum spaces. For the grid of $N+1$ equally spaced points $x_i=\Delta i$ $(i=0,...,N)$ these operations are given by

$$C_k=\alpha_k\sum_{m=0}^{N}\alpha_m F_m\cos(\pi mk/N),\quad k=0,...,N, \tag{20a}$$

$$F_m=\alpha_m\sum_{k=0}^{N}\alpha_k C_k\cos(\pi mk/N),\quad m=0,...,N, \tag{20b}$$

and

$$S_k=\alpha_k\sum_{m=0}^{N}\alpha_m F_m\sin(\pi mk/N),\quad k=0,...,N, \tag{21a}$$

$$F_m=\alpha_m\sum_{k=0}^{N}\alpha_k S_k\sin(\pi mk/N),\quad m=0,...,N, \tag{21b}$$

where the α_i coefficients are defined by Eq. (7). Compared to the standard way of writing of the direct and inverse sine transform we have added the zero components to the **S** and **F** vectors in Eqs. (21). These are S_0, S_N, F_0, and F_N. Similarly to Sec. II A, this only serves to get a compact formulation of the discrete form of the Laplacian operator. In discrete coordinate representation the V and Laplacian operators are given by $(N-1)\times(N-1)$ matrixes corresponding to $x_i=\Delta i$ $(i=1,...,N-1)$. The potential energy operator is given by a diagonal matrix: $V_{kn}=V(x_k)\delta_{kn}$ $(k,n=1,...,N-1)$. The Laplacian operator matrix has to be calculated numerically. Analogous to Eq. (11) it is obtained from

$$L_{kn}=-[\sqrt{\mathbf{B}}(\mathbf{A}_{\sin})^{-1}\mathbf{K}\mathbf{A}_{\cos}\mathbf{B}(\mathbf{A}_{\cos})^{-1}\mathbf{K}\mathbf{A}_{\sin}\sqrt{\mathbf{B}}\boldsymbol{\Xi}(\mathbf{n})]_k \quad (k,n=1,...,N-1). \tag{22}$$

The direct and inverse transforms are defined by Eqs. (20) and (21), **K** is the diagonal matrix given by Eq. (13). The $\boldsymbol{\Xi}(\mathbf{n})$ vector is defined as $\Xi(n)_i=\delta_{in}$ $(i=0,...,N)$. The diagonal matrices **B** and $\sqrt{\mathbf{B}}$ are given by

$$B_{ij}=\frac{1}{J(x_i)}\delta_{ij},\quad \text{and}\quad (\sqrt{B})_{ij}=\frac{1}{\sqrt{J(x_i)}}\delta_{ij}\quad (i,j=0,...,N). \tag{23}$$

The discretization procedure presented here results, as in the case of cylindrical coordinates, in a real and symmetric (Hermitian) Hamiltonian matrix.

The mapping function $r=f(x)$ is calculated along the lines discussed in Sec. II B. As the exponential-like variable change close to the origin is very efficient in describing the Coulomb wave functions,[23,24] we take the generating potential equal to

$$U(r)=-\frac{1}{4(r+\epsilon)^2}-\frac{Q}{r+\epsilon}. \tag{24}$$

The 1/4 coefficient in the first term is an adjustable parameter.

B. Results

Since we are interested in the Rydberg series of states, the W parameter in Eq. (15) was set equal to zero. All results presented below correspond to the mapping function $f(x)$ obtained from Eq. (15) with the generating potential given by Eq. (24) and with the parameter values $\Delta=1$ and $\alpha=1/1.5$. In Fig. 5 we show the results obtained with $N=96$ for different nucleus charges. More than 30 eigenstates could be obtained for all cases with an extremely good precision which is several orders of magnitude better to the one obtained with analytical mapping.[17] Through the only change of the nucleus charge Q in the generating potential the mapping procedure is automatically readjusted to the problem at hand. This makes the present approach a potentially very valuable tool for electronic structure calculations. The FGH method with numerical mapping reported by Kokoouline and Kosloff[23] leads to comparable results with a slightly lower precision if nonsymmetric form of Laplacian operator is used leading to a non-Hermitian Hamiltonian matrix. The symmetrization of the Laplacian operator performed in Ref. 23 results in a precision lower by two orders of magnitude than the one obtained in the present approach. This loss of precision comes from the extra-potential terms used to derive the symmetric form of the Laplacian operator (see discussion in Refs. 21 and 23).

In Fig. 6 we present an analysis of the sampling efficiency for the case of the Ar^{18+}. The sampling efficiency η is defined as the number N_e of converged eigenstates representable on the grid divided by the number N of the grid

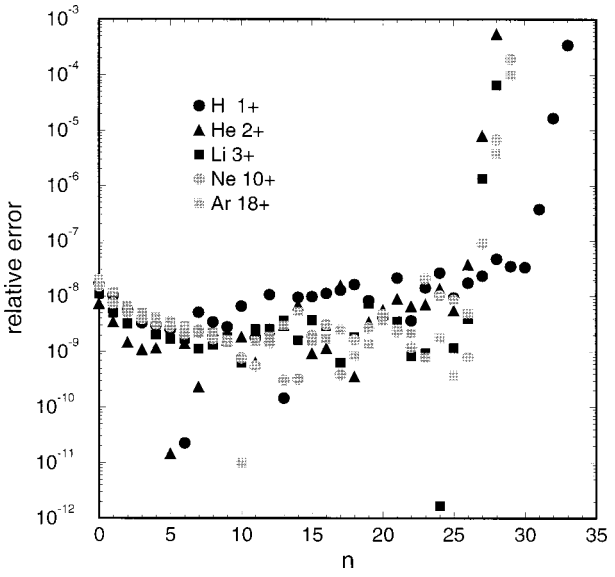

FIG. 5. Radial Schrödinger equation in spherical coordinates. Relative error in the eigenvalue calculation for the states of *s*-symmetry ($l=0$) as function of the radial quantum number *n* for different nucleus charges as presented in the inset of the figure. The calculation is performed with $N=96$ points on the grid. Δ, α, and W are parameters that are defined in the text.

points: $\eta=N_e/N$.[17] Here N_e corresponds to the number of states calculated with a precision of seven significant figures or better. At small N the sampling efficiency quickly increases with increasing N and saturates at approximately 45% level for large N. This corresponds to 2 grid points needed per converged eigenstate. The explanation for low sampling efficiency at small N is the same as for the cylindrical coordinate case. For a given N, a fixed number N_0 of grid points is required to describe the fast variation of the wave function close to the nucleus. At larger distances from the nucleus the points on the physical grid are distributed in a way that guarantees the optimal representation of the local de Broglie wavelength. Therefore, the efficiency of the method is increased if large extensions L of the physical grid $0<r<L$ are of interest. The constant and high sampling efficiency for large N is a clear advantage of the numerical mapping over the analytical one.[17]

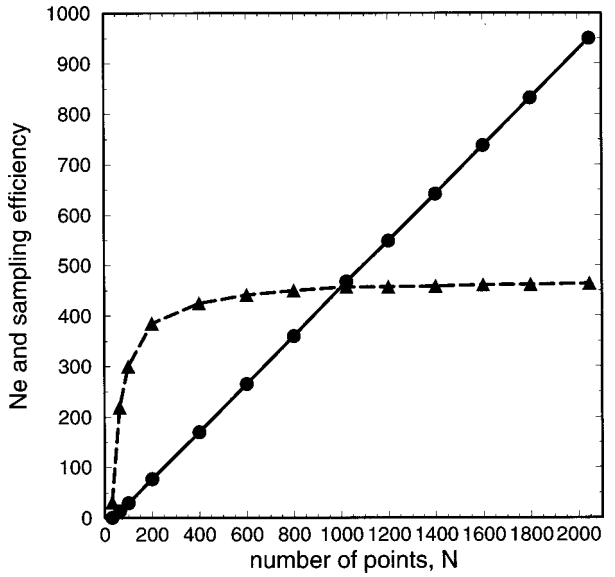

FIG. 6. Radial Schrödinger equation in spherical coordinates. Number of converged eigenstates N_e of *s*-symmetry ($l=0$) and sampling efficiency η as functions of the number N of grid points for the Ar^{18+} case. Solid line with black dots, number of eigenstates N_e obtained with at least seven significant figures. Dashed line with triangles, sampling efficiency $\eta=N_e/N$ ($\times 1000$).

IV. CONCLUSIONS

We have presented an efficient coordinate mapping procedure for both cylindrical and spherical geometries. The method outlined here is based on a numerical mapping, which sets an optimal distribution of the points on the physical grid allowing the precise description of the sought wave function. In contrast to earlier approaches, the highly symmetric representation *without* expanding the Laplacian operator is used. This removes the necessity of symmetrization procedure, which involves often rapidly varying extra-potential terms.[21–24] Therefore, the convergence of the eigenvalue calculation is improved. The Hamiltonian matrix is real and symmetric (Hermitian) and has to be calculated numerically, which can be easily done since the method readily exploits the fast sine and cosine transforms. Hermiticity of the Hamiltonian matrix allows one to use efficient diagonalization techniques for the eigenvalue solvers. Moreover, the present approach can be used in wave packet propagation treatments of time-dependent problems. The efficiency of the algorithm has been demonstrated for the 2D harmonic oscillator and 2D Coulomb problems as well as for the 3D Coulomb problem that can be of interest, e.g., for electronic structure calculations.

ACKNOWLEDGMENTS

The author is indebted to F. Aguillon, J. P. Gauyacq, and D. Lemoine for careful reading of the paper and valuable suggestions and comments. Illuminating discussions with V. Kokoouline are gratefully acknowledged.

[1] *Numerical Grid Methods and Their Applications to the Schrödinger Equation*, NATO ASI Series, Series C: Mathematical and Physical Sciences, edited by C. Cerjan (Kluwer Academic, Dordrecht, 1993), Vol. 412.
[2] J. V. Lill, G. A. Parker, and J. C. Light, Chem. Phys. Lett. **89**, 483 (1982).
[3] R. W. Heather and J. C. Light, J. Chem. Phys. **79**, 147 (1983).
[4] J. C. Light, in *Time Dependent Quantum Molecular Dynamics*, NATO ASI Series, Series B: Physics, edited by J. Broeckhove and L. Lathouwers (Plenum, New York, 1992), Vol. 299, p. 185.
[5] M. D. Feit, J. A. Fleck, Jr., and A. Steiger, J. Comput. Phys. **47**, 412 (1982).
[6] D. Kosloff and R. Kosloff, J. Comput. Phys. **52**, 35 (1983).
[7] R. Kosloff, in *Time Dependent Quantum Molecular Dynamics*, NATO ASI Series, Series B: Physics, edited by J. Broeckhove and L. Lathouwers (Plenum, New York, 1992), Vol. 299, p. 97.
[8] Geert-Jan Kroes, Prog. Surf. Sci. **60**, 1 (1999).
[9] D. Luckhaus, J. Chem. Phys. **113**, 1329 (2000).
[10] N. Rom, J. W. Pang, and D. Neuhauser, J. Chem. Phys. **105**, 10436 (1996).
[11] T. N. Rescigno and C. W. McCurdy, Phys. Rev. A **62**, 032706 (2000).
[12] V. A. Mandelshtam and H. S. Taylor, J. Chem. Phys. **102**, 7390 (1995).
[13] D. Colbert and W. H. Miller, J. Chem. Phys. **96**, 1982 (1992).
[14] R. Kosloff, J. Phys. Chem. **92**, 2087 (1988).
[15] C. C. Marston and G. G. Balint-Kurti, J. Chem. Phys. **91**, 3571 (1989).
[16] M. Monnerville and J. M. Robbe, J. Chem. Phys. **101**, 7580 (1994).

[17] E. Fattal and R. Kosloff, Phys. Rev. E **53**, 1217 (1996).
[18] F. Gygi, Europhys. Lett. **19**, 617 (1992); Phys. Rev. B **48**, 11692 (1993).
[19] E. Tiesiga, G. J. Williams, and P. S. Julienne, Phys. Rev. A **57**, 4257 (1998).
[20] J. M. Pérez-Jordá, Phys. Rev. A **52**, 2778 (1995).
[21] D. Lemoine, Chem. Phys. Lett. **320**, 492 (2000).
[22] V. Kokoouline, O. Dulieu, R. Kosloff, and F. Masnou-Seeuws, J. Chem. Phys. **110**, 9865 (1999).
[23] V. Kokoouline and R. Kosloff (unpublished).
[24] I. Tuvi and Y. B. Band, J. Chem. Phys. **107**, 9079 (1997).
[25] D. Lemoine, Comput. Phys. Commun. **99**, 297 (1997).
[26] D. Lemoine, J. Chem. Phys. **101**, 3936 (1994).
[27] D. Lemoine, Chem. Phys. Lett. **224**, 483 (1994).
[28] W. H. Press, S. A. Teukolsky, W. T. Vetterling, and B. P. Flannery, *Numerical Recipies in Fortran* (Cambridge University Press, Cambridge, 1992).
[29] *Compaq Extended Math Library Reference Guide* (Compaq Computer Corporation, Houston, TX, 1999).
[30] R. Meyer, J. Chem. Phys. **52**, 2053 (1970).